International Journal of Engineering

Journal Homepage: www.ije.ir

Experimental and Numerical Investigation of the Formability of Cross and Accumulative Roll Bonded 1050 Aluminum Alloy Sheets in Single Point Incremental Forming Process

M. Mahmoodi*[a], H. Tagimalek[a], M. R. Maraki[b], S. Karimi[a]

[a] *Faculty of Mechanical Engineering, Semnan University, Semnan, Iran*
[b] *Department of Materials and Metallurgy Engineering, Birjand University of Technology, Birjand, Iran*

PAPER INFO

Paper history:
Received 08 March 2022
Received in revised form 14 April 2022
Accepted 18 April 2022

Keywords:
Single point incremental forming
Accumulative roll-bonding
Cross accumulative roll-bonding
Thickness Distribution
Formability
Force

ABSTRACT

As one of the methods of Severe Plastic Deformation (SPD), the Accumulative Roll-Bonding (ARB) process leads to the production of high-strength metal sheets and fine-grained structures. In this paper, the Single Point Incremental Forming (SPIF) of Al1050 sheets, processed by the ARB and CARB (Cross-Accumulative Roll-Bonding), is experimentally and numerically investigated. The forming force, thickness distribution, and forming depth in both cases (ARB and CARB) are all determined in this research. The result shows that the formability of CARB samples is higher than ARB samples. Furthermore, the formability of both ARB and Al1050 annealed samples are equal in the initial pass. In addition, the samples' strain is enhanced by increasing the number of rolling passes, and as a result, the formability scales down. The results obtained using the dynamometer reveals that the vertical forming force extent in the CARB samples is higher than the rest of the samples.

***doi**: 10.5829/ije.2022.35.09c.05*

1. INTRODUCTION[1]

Al 1050, due to its high corrosion resistance, good formability, high electrical and thermal conductivity, and high weldability, has been considered [1, 2]. Besides, with an increasing development of the industry, the processes of severe plastic deformation are important as an effective method for the production of high-strength metals and ultra-fine structures [3, 4]. Incremental sheet process is a new process for metal sheet forming in low-volume production without making a die [5]. Advantages of this method include formability, numerical process control capability, and low cost of equipment [6, 7]. The incremental forming is generally divided into two categories: single-point incremental formation (SPIF) and two-point incremental formation (TPIF) [8]. One of the main components in the SPIF is the sheet material and several studies have been conducted in this regard [9, 10]. Najm et al. [11] in order to produce a SPIF component with sufficient quality without defects, selected the optimal process parameters. In other work [12] they investigated the effects of forming tool characteristics on the accuracy and formability of thin aluminum alloy blanks when using SPIF. Paniti et al. [13] by monitoring servo-motor currents, estimated the forming force in the SPIF and gave a new crack monitoring method based on light sensor.

Suresh et al. [14] examined the effect of the tool path on the incremental sheet process. They found several ways to choose a tool path in the incremental sheet process, and the most important parameters of the tool path were the vertical step, the length of the tool path, and the number of passes that indicate the better formability of the sheet. By reducing the percentage of thinning of the sheet in the direction of the circular tool, the formability will increase. Jackson et al. [15] practically examined the possibility of substituting sheet incremental formwork for sandwich panels. The feasibility of the process was performed by examining the states of thinning, failure, and surface quality after the incremental forming process for different patterns of sandwich panel. Three groups of panels (metal/metal fiber/metal, metal/polymer/metal and metal/metal foam/metal) were examined. Incremental forming can be used successfully to form sandwich panels with metal foam core. Nikdooz et al. [16] examined the two-step incremental formation of an incomplete 70-degree square pyramid to improve the minimum thickness. They found that using a two-

*Correponding author institutional Email: mahmoodi@semnan.ac.ir (Masoud Mahmoodi)

Please cite this article as: M. Mahmoodi, H. Tagimalek, M. R. Maraki, S. Karimi, Experimental and Numerical Investigation of the Formability of Cross and Accumulative Roll Bonded 1050 Aluminum Alloy Sheets in Single Point Incremental Forming Process, ***International Journal of Engineering, Transactions C: Aspects***, Vol. 35, No. 09, (2022)

step strategy could double the minimum thickness by a single step. Lu et al. [17] designed a new tool for increasing the shape of aluminum sheets with different alloys. At the tip of the tool, an indirect ball bearing is located. It is possible to prevent the contact of the upper areas of the tip of the tool, which causes the highest friction in the sheet, and improves the formability.

Najm et al. [18] investigated the best results of the final geometry, thickness homogeneity, minimum pillow surface, and maximum forming depth using different shapes and different sizes of the tool.

Neto et al. [19] presented a complete finite element model to examine the stress and strain state near the contact surface. They found that the small contact surface between the tool and the sheet had a positive effect on the stresses under the tool, which delayed the soft failure. It was also concluded, the residual stresses in both circumferential and meridional directions are positive in the inner skin of the cone and negative in the outer skin. Hino et al. [20] studied the effect of grain size on Al 1050 rolled sheets on the vertical forming force. In the results shown, the curvature trend is similar for almost all samples, except that the peak value of the forming force increases with decreasing grain size, which is due to the large displacement density of the coarse grains. Mansouri et al. [21] have investigated the microstructure of the ARB method of sandwich sheets using stainless steel, copper, and aluminum. The analysis showed that in the first and second passes of the ARB, no plastic instability was created in the layers. With the increase in the number of passes of the accumulative roll bonding, plastic instability and eventually fracture will be observed. According to the results of this study, during the ARB process, a proper bonding has been established between the layers. Rahmatabadi et al. [22] studied Young's modulus, the anisotropy coefficient in the rolling direction, and other elastic and plastic parameters of multilayer aluminum /brass composite produced by ARB process. The results showed that a good relation between aluminum /brass mixing in the original sandwich was made and strengthened by increasing the stability pressure. In the other work [23], they examined the effect of the ARB process on the fracture toughness of ultrafine-grained aluminum. Test results showed that by increasing the number of the ARB cycles, fracture toughness was increased and the maximum value of this parameter achieved in the last cycle.
Past Researches in the SPIF process were on single-layer and multilayer sheets. Due to the capabilities of the SPIF process and the properties of the multilayer sheets, it can be used to produce parts with multilayer sheet.

In this paper, the incremental single point forming of Al 1050 sheets processed by the ARB and CARB has been studied experimentally and numerically. The effect of the ARB and CARB process and heat-treatment on the formability of the samples and forming forces were investigated.

2. MATERIALS AND METHODS

2.1. ARB experiments

The 1050 aluminum sheets were bonded by the ARB and then formed by the SPIF process. The thickness of the sheet used was 1 mm, with dimensions of 130 × 130 $mm^{2,}$ and cut according to the size of the die. The chemical composition of the Al 1050 sheet obtained from quantometry analysis, are summarized in Table (1).

Table 1. Chemical composition of Al 1050

Metal	Al	Zr	V	Sr	Pb
Al 1050	99.54	0.0137	0.0164	0.002	0.0044
Ti	**Sn**	**Ni**	**Cr**	**Mn**	**Fe**
0.0044	0.009	0.0019	0.0066	0.010	0.157

The use of rolling in the ARB process is not only as a deformation method but also as a factor for creating bonding between two sheets and producing a completely integrated sheet. To increase the adhesion of the layers, the accumulative roll-bonding process was done in the cold and non-lubricating conditions. In the ARB process, the sever plastic deformation produces a solid-state bonding. According to the Film theory, as a dominant mechanism of low temperature ARB, bonding occurs when metal surfaces are exposed and deformed to a sufficiently large value. The fracture of surface layers and extrusion of virgin metals through the cracks have the main roles in a real contact. The reduction percent at this stage was 50%, and as a result, the thickness of the sheet was equal to the thickness of the original sheet. Then the sheet was cut in two lengthwise, and the steps are repeated. Fig. (1) shows a schematic of the ARB and CARB process. The number of layers of sheet bonded by the ARB method was obtained from the relation 2^n(n is the number of passes). The ARB processed sample had 32 layers and the thickness of each layer was 31 µm.

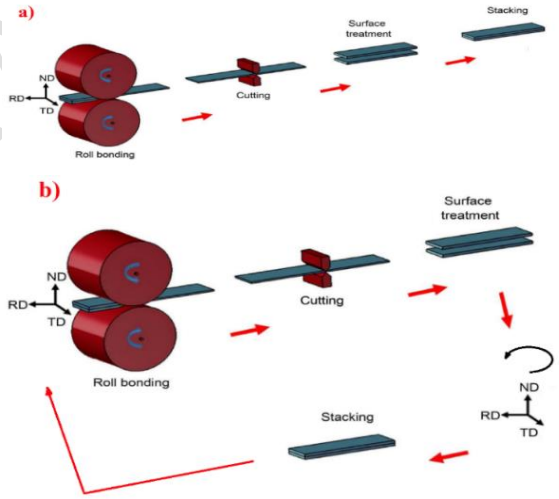

Fig. 1. Schematic of the bonding process; a) ARB, and b) CARB

2.2. SPIF experiments

In the empirical test of ISF, the rotational speed of the tool was 900 RPM, the forward speed was 700 mm/min, and the vertical step was 0.5 mm.

In the SPIF process, it is necessary to control the sheet. Fig. (2) shows the tools and fixtures used for the SPIF process. Table (2) shows the specifications of the experimental test samples. According to Table 2, Al 1050, 1ARB, 3ARB, 5ARB and 3CARB samples were annealed at 380°C for 60 minutes. To perform the tensile tests, samples were prepared according to standard ASTM E8-04 [24].

Table 2. Specifications of experimental samples

Type	Number of passes	Heat-treatment	Code
Al 1050	--	*	Anneal Al 1050

ARB	1	*	1ARBH
ARB	3	*	3ARBH
ARB	5	*	5ARBH
ARB	1	--	1ARB
ARB	3	--	3ARB
CARB	3	--	3CARB
CARB	3	*	3CARBH

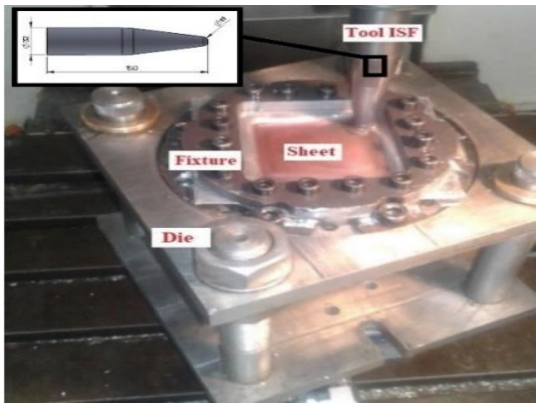

Fig. 2. Tools and fixtures used for the SPIF process

To apply ISF, a spherical VCN alloy steel head tool with a diameter of 11 mm and hardness of 25 HRC was used. To ensure better performance and prevent sudden failure, and non-corrosion of the tip of the tool, it was heated at a temperature of +950°C and cooled in oil. To perform the SPIF process, it's necessary to move the tool simultaneously in a specific direction in three directions X, Y, and Z. Therefore, the John Ford VMC-850 three-axis CNC milling machine was used for the SPIF process.

Tensile test was performed by the machine SANTAM STM-150 in Semnan University. A dynamometer with piezoelectric b9257 was used to measure the force. The SPIF process and then the measurement of the depth of tension was done by the CNC machine John Ford VMC-850 three-axis CNC milling made in Taiwan country. According to Fig. (3), the path selected in this study is a square path, and the tool must move in a steady direction along the Z-axis and form the sample.

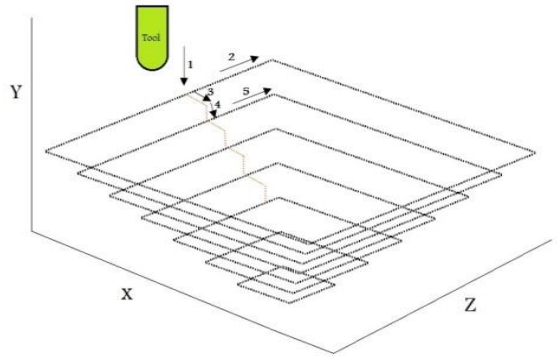

Fig. 3. The tool path for the SPIF process

Two common paths have been used in ISF are profile tool path and spiral tool path. Many previous studies proved that the spiral path strategy shows better results than the profile path in formability, geometric accuracy, and surface roughness of ISF components. But in this work, according to the square shape of the sample, the unidirectional profile tool path was designed based on Jadhav's work [25]. He observed twist and dent in parts formed using spiral tool path. The numerical control program to introduce the square path of the process was created by MATLAB. After fixing the sheet on the fixture and preparation of the CNC milling machine, SPIF was done.

To measure the thickness distribution, the part's thickness was determined at different points using an ultrasonic thickness gauge with an accuracy of 0.01 mm in a cross section along the middle plane that for all the forming depth could be different. Song et al. [26] showed there was three different zones along the components wall of ISF (bending/stretching, shear, and stretch/shear). The thickness distribution includes these areas.

3. FINITE ELEMENT ANALYSIS

To simulate the SPIF process, Abaqus finite element software was used, and the FE model shown in Fig. (4). The tools and die were considered to be analytical rigid. The material behavior was considered to be Elastic-Plastic, and assumed that follow the Von-Mises yield criterion. The blank sheet was meshed using for node shell elements with reduced integration (S4R). All surface-to-surface contacts were selected by mechanical contact with tangential behavior in the Columbus friction model. The friction coefficient was 0.1. To simulate the ISF process, Abaqus 2019 software was used. The contact between the backup plate and the sheet was defined as frictionless and wholly constrained. In this modeling, the written code in MATLAB software was used to move the tool. Then the output of this program is defined as a domain in Abaqus software that specifies the tool's movement in all three directions X, Y, and Z at any time. Therefore, due to the large deformation in the cold state process, a dynamic explicit solvent was used.

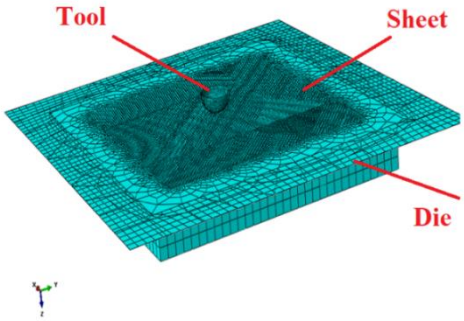

Fig. 4. FE model of the SPIF process in Abaqus software

To obtain the optimal mesh size, the effect of mesh size on the equivalent plastic strain (PEEQ) was investigated. Fig. (5) shows the effect of the mesh size on PEEQ from the sample center.

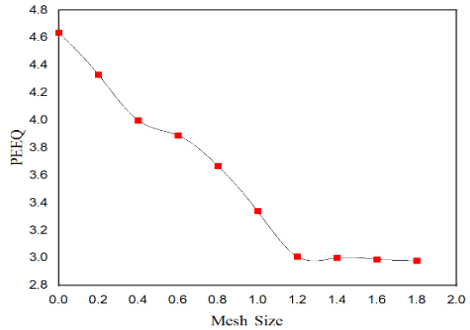

Fig. 5. Mesh Sensitivity Diagram: Effect of mesh size on the equivalent plastic strain of Al 1050 sample

So, the mesh size of 1.2 was used to simulate the sheet. In this study, the purpose of the simulation was to investigate the validity of the results in ARB samples that underwent the SPIF process. In FE analysis, only data from existing ARB samples were examined.

4. RESULTS AND DISCUSSION

Because the ARB process is an SPD process, the plane strain rolling process produces different properties in different directions of the sheet. Therefore, due to the anisotropy, different properties are obtained in the directions of RD, TD and 45-degree rolling. Therefore, the tensile test results were evaluated on seven existing samples in three transverse, longitudinal, and 45-degree positions relative to the rolling direction. Fig. (6) shows the stress-strain curves of the ARB samples at three different directions 0°, 45°, and 90° angle to the rolling direction. The tensile strength of ARB samples, according to this figure, compared to the annealed sheet has increased, and the formability has decreased. To simulate the finite element and define the properties of materials, it was necessary to have true stress and strain of the material, so the engineering stress-strain obtained from the tensile test must be converted to a true stress-strain. To evaluate the forming forces, a dynamometer with piezoelectric b9257 and amplifier identification number 6019b126 was used to measure the main vertical forces. By putting the die on the dynamometer and performing the SPIF process, the tool's forces could be obtained in three directions. The most significant effect of the force in the SPIF process was in the vertical direction, so only the vertical force was studied. Fig. (7) shows the force applied to the tool before filtering. As shown in the figure, the amount of forming force increases until it reaches the necking point, and then due to strain hardening with the thinning defect, a decrease in force was observed.

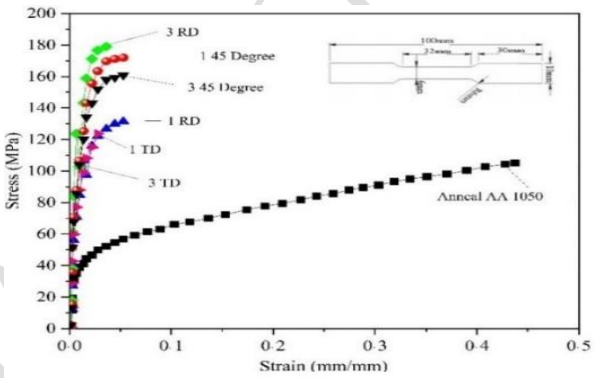

Fig. 6: True stress-strain curves after the ARB process

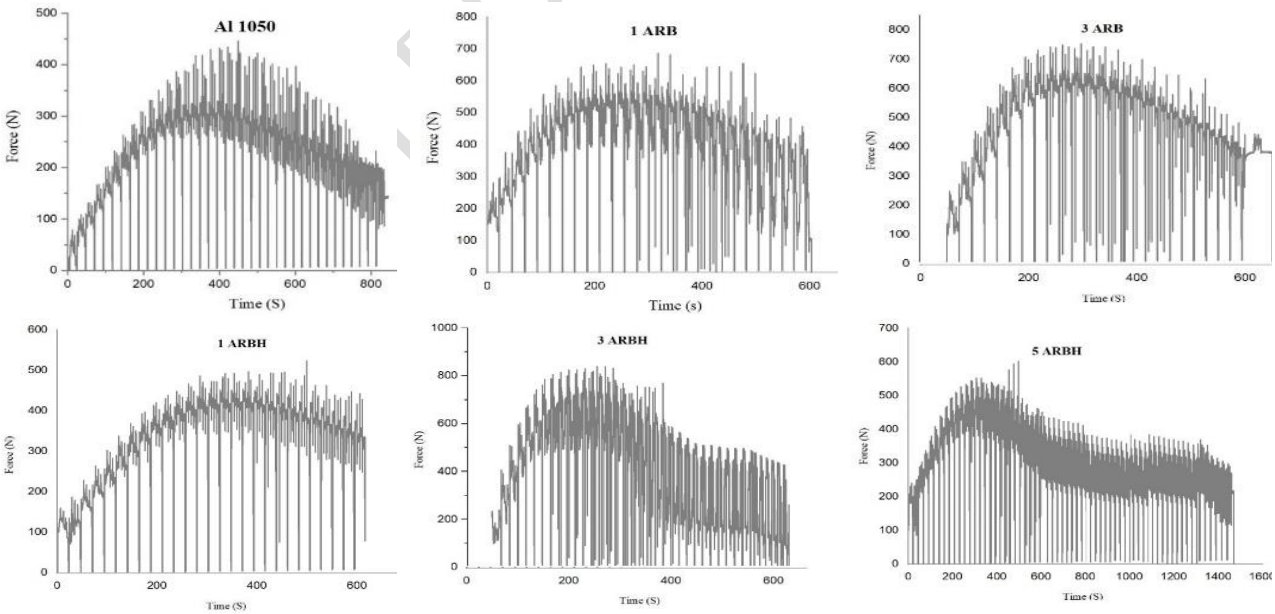

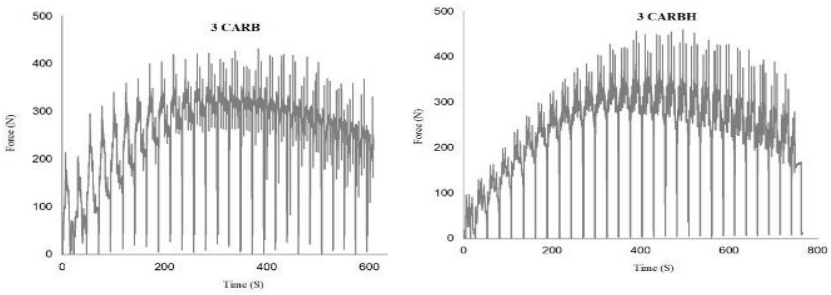

Fig. 7. Vertical forming force in the SPIF process (Measured by Dynamometer with piezoelectric b9257 before filtering)

Because the behavior of materials is different in all samples of experimental designs, their formability is also different during the ISF process. As shown in the results, they experience different formability and forming depth. Therefore, the degree of formability and the process continuity affect the time and also the extreme force occurs at different times. The purpose of using a dynamometer is to reach the extreme of force. The ARB process' impact on the forming force is depicted in Fig. (8). Increased the number of passes in the ARB process, the tensile strength promotes very rapidly in the first pass. The rise of pass number heightens the sheets' tensile strength, and thus, the forming force in the SPIF process aggravates. The samples' tensile strength is reduced by the annealing heat-treatment, so it devaluates the forming force significantly. In all similar passes, the CARB sheets' tensile strength is higher than ARB sheets', and consequently, the CARB sheets are of greater SPIF forces. As a result, the samples' forming force is declined as compared to the samples without heat-treatment, so that the force in a one-pass ARBH sample is subtracted up to 18% as compared to a one-pass ARB sample. Moreover, a 47% reduction in force is observed in a three-pass ARB sample as compared to its equivalent sample, which imposed to the heat-treatment. In case of a three-pass CARB sample, a 5% increment has been observed in forming force as compared to a three-pass ARBH sample. As well, in a three-pass CARB sample as compared to a one-pass ARBH sample, the force is increased by 25%. This force augmentation is due to the higher tensile strength of CARB sheets than ARB in each similar cycle [20]. As shown in Fig. (8), the simulative results are in a good agreement with the experimental results.

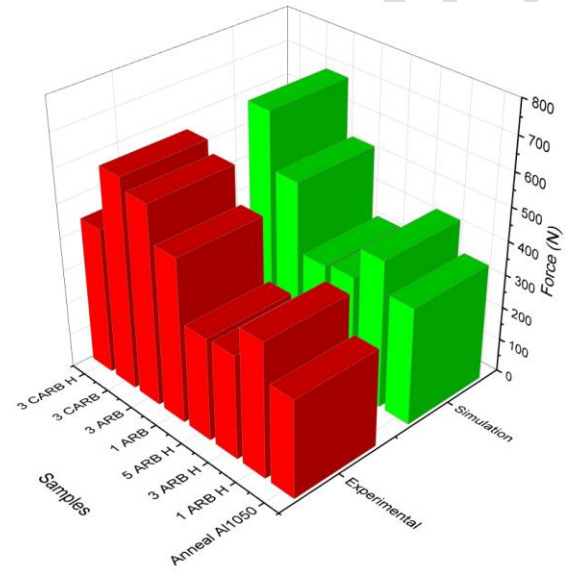

Fig. 8. Experimental and numerical comparison of the forming forces in samples

Fig. (9) shows the different experimental samples formed by the SPIF process. The localized necking occurs in some processes, such as incremental forming in areas of metal that there is plane stress and also normal stress. In this study, the localized necking criteria were used. The presence of normal stress in the incremental forming process leads to the improvement of the formability of the material and, as a result, the surface of the forming limit curve is higher.

Fig. 9: Samples produced by experimental SPIF processes

The presence of normal stress reduces the forming loads in the positions of geometric heterogeneity from which failure begins. Fig. (10) shows the onset of a localized necking before complete failure.

Fig. 10: Onset of localized necking

The thickness of the samples produced from the longitudinal section was measured by an ultrasonic thickness gauge. Fig. (11) shows the path for measuring the thickness distribution. Thickness measurements in experimental samples and simulation after sheet fracture were performed at maximum forming depth. By applying the mechanical properties of the samples and performing simulations in ABAQUS finite element software, the results obtained were compared with the experimental results.

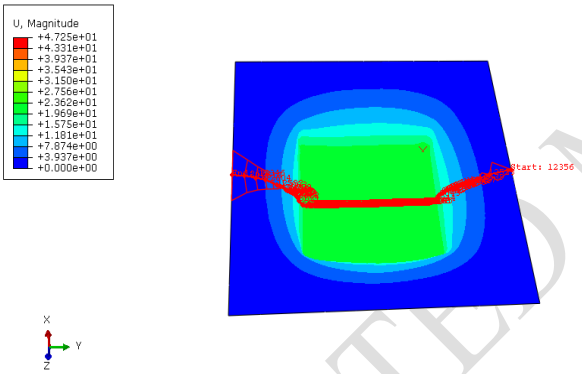

Fig. 11. The path of measured thickness in the FE model

The simulation results in the samples are in good agreement with the experimental results. Besides, the simulation results show relatively accurate changes in the location of the thinnest thickness.

In the thickness distribution discussion, the most significant difference between the simulation results and the experimental results was 9.4% (3ARB). Since by applying the ARB process on the Al 1050 sample, a considerable strain is applied to the sample in each pass; therefore, the samples become more brittle. As shown in Fig. (12), in the 1ARB sample the thickness of the fracture area was 0.30 mm, which was 0.38 mm thick compared to the 3ARB sample.

Performing heat-treatment on the samples and a significant reduction in sheet thickness at the point of the fracture indicates an improvement in the formability properties of the samples affected by heat-treatment. As shown in Fig. (13), the fracture thickness of the 1ARBH sample was 0.38 mm, which was 0.08 mm different from the non-heat treated one. This difference indicates that by applying heat treatment, the percentage of thinning of the sheet increases and also improves the formability of the samples. Comparing the diagrams shows increasing the number of ARB passes increases the thickness of the sheet at the fracture point.

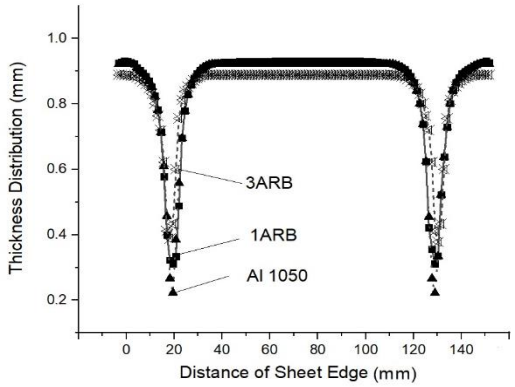

Fig. 12. Thickness distribution curve in the ARB samples

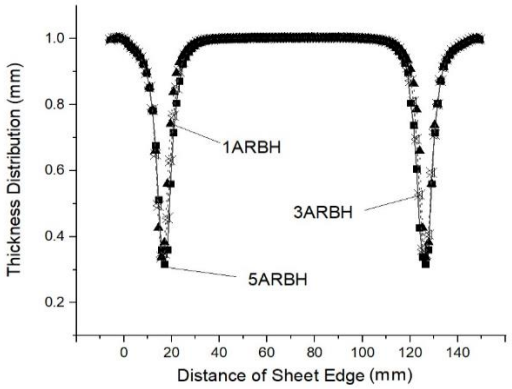

Fig. 13. Thickness distribution curves in the heat-treated ARB samples

Fig. (14) shows the thickness distribution profile of the sample produced in the CARB process using an ultrasonic thickness gauge. The minimum thickness of the 3CARB sheet was 0.35 mm, which is 0.03 mm different from the 3ARB sheet. The results of the thickness distribution profile show that the amount of thinning was more significant than the ARB samples.

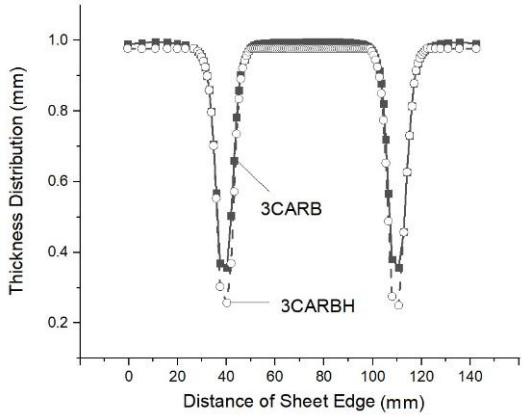

Fig. 14. Thickness distribution curves in the heat-treat CARBed sample

The profile of the wire cut machining sample was determined using a projector profile machines with an accuracy of 0.001 mm. Fig. (15) shows the cross-section depth profiles of the samples formed by the SPIF method. At the beginning of the profiles of the samples were curved due to the flow of the sheet, and then due to the Spring back phenomenon, they have an angle of fewer than 80 degrees. The formability of the 3CARBH sample (3 passes CARB with heat-treatment) was higher than other samples. Many grain boundaries acted as a barrier to the growth of the main crack and provided better CARB formability. Also, the formability of the 3ARBH sample was higher than the Al 1050 sample. The 3ARB sample also has the lowest formability due to the brittleness of the sheet in the ARB process. It should be noted that the floor thickness of the formed profiles is constant.

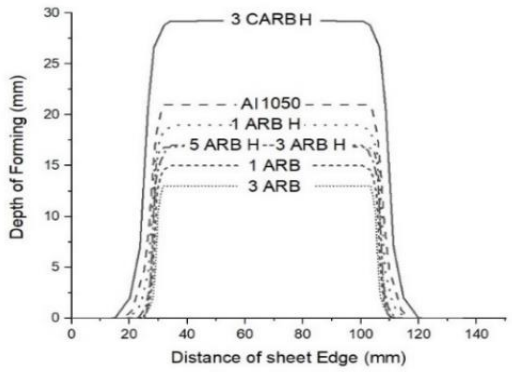

Fig. 15. Depth profiles of formed samples by the SPIF process

To find the height of the breaking point, there are two methods: 1. Position display on the CNC screen, 2. Recording by Dynamometer. After the sheet fractures, the dynamometer was disconnected, and the fracture time was recorded. Using this time, the breaking point height can be obtained in Power mill software. Fig. (16) shows the maximum forming depth of the samples at the SPIF process. As can be seen, the formability of the 3CARBH sample is 29 mm, which is significantly different from other samples (Maximum forming depth is 29 mm). Also, the formability of CARB samples is higher than that of ARB samples. The formability of CARB samples is more exorbitant than that of ARB samples. Therefore, a great deal of grain boundaries acts as a barrier to the main crack growth and causes better CARB formability, so that the CARB samples' formability is higher than Al1050 [27].

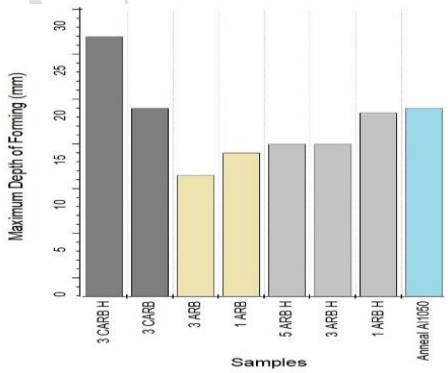

Fig. 16. Diagram of the Maximum SPIF depth of the samples

5. CONCLUSIONS

In this paper, the SPIF of Al1050 sheets, processed by both the ARB and CARB, is studied. The results of this study are as follows:

- In the ARB process, the severe strain is applied to the sample: it causes the grains to become finer, and the sample to become more brittle. Therefore, the ARB samples' formability is less than that of Al1050 sheets.
- The samples' formability is improved by the heat-treating of ARB and CARB samples.
- Each pass in the ARB process increases the sheet's tensile strength, because of which the forming force of these sheets in the SPIF process is also intensified.
- The tensile strength of CARB sheets is higher than ARB sheets in any similar pass, so the SPIF force of CARB sheets is more eminent.
- The formability of CARB samples is more exorbitant than that of ARB samples. Therefore, a great deal of grain boundaries acts as a barrier to the main crack growth and causes a better CARB formability, so that the CARB samples' formability is higher than Al1050.
- For further investigation, the DOE technique could be adopted to decrease the sample size, estimate the effect of each parameter and get the better results.

6. REFERENCE

1. Trzepiecinski, T., Najm, S.M., Oleksik, V., Vasilce, D., Paniti, I., and Szpunar, M., "Recent developments and future challenges in incremental sheet forming of aluminium and aluminium alloy sheets", ***Metals***, Vol. 12, No. 1, (2022) :124. https://doi.org/10.3390/met12010124.
2. Bagherzadeh, S., Abrinia, K. and Han, Q., "Analysis of plastic deformation behavior of ultrafine-grained aluminum processed by the newly developed ultrasonic vibration enhanced ECAP: simulation and experiments", ***Journal of Manufacturing Processes,*** Vol. 50, pp. 485-497, (2020). https://doi.org/10.1016/j.jmapro.2020.01.010.
3. Maraki, M.R., Tagimalek, H, and Pasoodeh, B., "Provide a modeling algorithm for mechanical properties of friction stir welding of 5 series aluminum and pure-copper based on Fuzzy logic," ***Iranian (Iranica) Journal of Energy and Environment***, Vol. 13, No. 2, pp.169-175, (2022). Doi:10.5829/ijee.2022.13.02.08
4. Lei, W. and Zhang, H., "Analysis of microstructural evolution and compressive properties for pure Mg after room-temperature ECAP," ***Materials Letters***, Vol. 271, 127781, (2020). https://doi.org/10.1016/j.matlet.2020.127781.
5. Tamimi, S., Gracio, J. J., Lopes, A. B., Ahzi, S. and Barlat, F., "Asymmetric rolling of interstitial free steel sheets: Microstructural evolution and mechanical properties," ***Journal of Manufacturing Processes***, Vol. 31, pp. 583-592, (2018). https://doi.org/10.1016/j.jmapro.2017.12.014.
6. Kyaw, P.M., Osawa, N., Gadallah, R. and Tanaka, S., "Accurate and efficient method for analyzing mixed-mode SIFs for inclined surface cracks in semi-infinite bodies by using numerical influence function method", ***Theoretical and Applied Fracture Mechanics***, Vol. 106, 102471, (2020). https://doi.org/10.1016/j.tafmec.2019.102471.
7. Tagimalek, H., Maraki, M.R., and Mahmoodi, M., "A new approach of the constrained groove pressing process on Al5083-O alloy using PMMA polymer, without die non-friction

coefficient: nanostructure, mechanical Properties and hardness", ***Journal of Engineering Research***, (2021). https://doi.org/10.36909/jer.12957.

8. Liavoli, R.P., Gorji, H., Bakhshi-Jooybari, M. and Mirnia, M.J., "Investigation on Formability of Tailor-Welded Blanks in Incremental Forming", ***International Journal of Engineering, Transactions B: Applications*** Vol. 33, No. 5, pp. 906-915, (2020). doi:10.5829/ije.2020.33. 05b.23.
9. Martínez-Donaire, A.J., Borrego, M., Morales-Palma, D., Centeno, G. and Vallellano, C., "Analysis of the influence of stress triaxiality on formability of hole-flanging by single-stage SPIF", ***International Journal of Mechanical Sciences***, Vol. 151, pp. 76-84, (2019). https://doi.org/10.1016/j.ijmecsci.2018.11.006.
10. Wang, Z., Cai, A. and Chen. J., "Experimental investigations on friction stir assisted single point incremental forming of low-formability aluminum alloy sheet for higher formability with reasonable surface quality", ***Journal of Materials Processing Technology***, Vol. 277, 116488, (2020). https://doi.org/10.1016/j.jmatprotec.2019.116488.
11. Najm, S.M., Paniti, I., Trzepiecinski, T., Nama, S.A., Viharos, Z.J. and Jacso, A., "Parametric effects of single point incremental forming on hardness of AA1100 aluminium alloy sheets", ***Materials***, Vol. 14, No. 23, 7263, (2021). https://doi.org/10.3390/ma14237263.
12. Najm, S.M. and Paniti, I., "Artificial neural network for modeling and investigating the effects of forming tool characteristics on the accuracy and formability of thin aluminum alloy blanks when using SPIF", ***The International Journal of Advanced Manufacturing Technology***, Vol. 114, pp. 2591-2615, (2021). https://doi.org/10.1007/s00170-021-06712-4.
13. Paniti, I., Viharos, Z.J., Harangozo, D. and Najm, S.M., "Experimental and numerical investigation of the single point incremental forming of aluminium alloy foils", ***ACTA IMECO***, Vol. 9, No. 1, pp. 25-31, (2020). http://dx.doi.org/10.21014/acta_imeko.v9i1.750.
14. Suresh, K., Khan, A. and Regalla, S.P., "Tool path definition for numerical simulation of single point incremental forming", ***Procedia Engineering***, Vol. 64, pp. 536-545, (2013). https://doi.org/10.1016/j.proeng.2013.09.128.
15. Jackson, K., Allwood, J. and Landert, M., "Incremental forming of sandwich panels", ***Journal of Materials Processing Technology***, Vol. 204, No. 1, pp. 290-303, (2008). https://doi.org/10.1016/j.jmatprotec.2007.11.117.
16. Nikdooz, A. H., Mirnia. M. J. and Baseri, H., "Study of formability of aluminum truncared pyramid in single-stagesnd two-stage incremental sheet forming," ***Modares Mechanical Engineering***, Vol. 16, No. 5, pp. 210-220, (2016). http://mme.modares.ac.ir/article-15-9274-en.html.
17. Lu, B., Fang, Y., Xu, D., Chen, J., Ou, H., Moser, N. and Cao, J., "Mechanism investigation of friction- related effects in single point incremental forming using a developed oblique roller-ball tool," ***International Journal of Machine Tools and Manufacture***, Vol. 85, pp. 14-29, (2014). https://doi.org/10.1016/j.ijmachtools.2014.04.007.
18. Najm, S. M. and Paniti, I., "Study on effecting parameters of flat and hemispherical end tools in SPIF of aluminium foils", ***Technical Gazette***, Vol. 27, No. 6, pp. 1844-1849, (2020). https://doi.org/10.17559/TV-20190513181910.
19. Neto, D.M., Martins, J.M.P., Oliveria, M.C., Menexes, L.F. and Alves, J. L., "Evaluation of strain and stress states in the single point incremental forming process", ***The International Journal of Advanced Manufacturing Technology***, Vol. 85, pp. 521-534, (2016). https://doi.org/10.1007/s00170-015-7954-9.
20. Hino, R., Kawabata, K. and Yoshida, F., "Incremental forming with local heating by laser irradiation for magnesium alloy sheet," ***Procedia Engineering***, Vol. 81, pp. 2330-2335, (2014). https://doi.org/10.1016/j.proeng.2014.10.329.
21. Mansouri, M., Eghbali, B. and Afrand, M., "Producing multi-layer composite of stainless steel/aluminum/copper by Accumulative roll-bonding (ARB) process," ***Journal of Manufacturing Processes***, Vol. 46, pp. 298-303, (2019). https://doi.org/10.1016/j.jmapro.2019.08.025.
22. Rahmatabadi, D., Shahmirzaloo, A., Farahani, M., Tayyebi, M. and Hashemi, R., "Characterizing the elastic and plastic properties of the multilayered Al/Brass composite produced by ARB using DIC," ***Materials Science and Engineering: A***, Vol. 753, pp. 70-78, (2019). https://doi.org/10.1016/j.msea.2019.03.002.
23. Rahmatabadi, D., Hashemi, R., Mohammadi, M. and Shojaee, T., "Experimental evaluation of the plane stress fracture toughness for ultra-fine grained aluminum samples prepared by Accumulative roll-bonding process," ***Materials Science and Engineering: A***, Vol. 708, pp. 301-310, (2017). https://doi.org/10.1016/j.msea.2017.09.085.
24. ASTM E8-04, Standard test method for tension testing of metallic materials. ASTM International.
25. Jadhav, S., "Basic Investigations of the Incremental Sheet Metal Forming Process on a CNC Milling Machine", Doctorate Thesis, University of Dortmund, Germany, (2004).
26. Song, X., Zhang, J., Zhai, W., Taureza, M., Castagne, S., Danno, A., "Numerical and Experimental Study of Micro Single Point Incremental Forming Process", ***Procedia Engineering***, Vol 207, pp. 825–830 (2017). https://doi.org/10.1016/j.proeng.2017.10.836
27. Roghani, H., Borhani, E., Shams, S.A.A., Lee. C.S. and Jafarian, H.R., "Effect of concurrent accumulative roll bonding (ARB) process and various heat treatment on the microstructure, texture and mechanical properties of AA1050 sheets," ***Journal of Materials Research and Technology***, Vol. 18, pp. 1295-1306, 2022. https://doi.org/10.1016/j.jmrt.2022. 03.001.

Persian Abstract

به عنوان یکی از روش‌های تغییر شکل شدید پلاستیک، فرآیند نورد تجمعی منجر به تولید ورق‌های فلزی با مقاومت بالا و سازه‌های ریزدانه می‌شود. در این پژوهش، شکل‌دهی افزایشی نطقه‌ای ورق، ورق‌های آلومینیوم ۱۰۵۰ فرآوری شده توسط نورد تجمعی و نورد تجمعی متقاطع به صورت تجربی و عددی بررسی شد. نیروی شکل‌دهی، توزیع ضخامت و عمق شکل‌دهی در هر دو حالت نورد تجمعی و نورد تجمعی متقاطع همگی در این پژوهش تعیین گردید. نتایج نشان می‌دهد که شکل‌پذیری نمونه‌های نورد تجمعی متقاطع بیشتر از نمونه‌های نورد تجمعی است. علاوه بر این، شکل پذیری هر دو نمونه آنیل شده نورد تجمعی و آلومینیوم ۱۰۵۰ در پاس اولیه برابر است. علاوه بر این، کرنش نمونه‌ها با افزایش تعداد عبور نورد افزایش می‌یابد و در نتیجه شکل‌پذیری کاهش می‌یابد. نتایج به دست‌آمده با استفاده از دینامومتر نشان می‌دهد که میزان نیروی شکل‌دهی عمودی در نمونه‌های نورد تجمعی متقاطع بیشتر از بقیه نمونه‌ها است.